

High Resolution Spectral Line Indices Useful for the Analysis of Stellar Populations

LINO H. RODRÍGUEZ-MERINO,¹ Y. D. MAYYA,¹ PAULA R. T. COELHO,² GUSTAVO BRUZUAL,³
STÉPHANE CHARLOT,⁴ ESPERANZA CARRASCO,¹ AND ARMANDO GIL DE PAZ⁵

¹*Instituto Nacional de Astrofísica, Óptica y Electrónica*

Luis Enrique Erro 1, Tonantzintla, Puebla, C.P. 72840, Mexico

²*Universidade de São Paulo, Instituto de Astronomia, Geofísica e Ciências Atmosféricas*

Rua do Matão 1226, 05508-090, São Paulo, Brazil

³*Instituto de Radioastronomía y Astrofísica, Universidad Nacional Autónoma de México,*

Morelia, Michoacán, C.P. 58090, Mexico

⁴*Sorbonne Université, CNRS, UMR7095, Institut d'Astrophysique de Paris, F-75014, Paris, France*

⁵*Universidad Complutense de Madrid, Departamento de Física de la Tierra y Astrofísica,*

Instituto de Física de Partículas y del Cosmos IPARCOS, E-28040, Madrid, Spain

(Received December 16, 2019; Accepted January 19, 2020)

ABSTRACT

The well-known age-metallicity-attenuation degeneracy does not permit unique and good estimates of basic parameters of stars and stellar populations. The effects of dust can be avoided using spectral line indices, but current methods have not been able to break the age-metallicity degeneracy. Here we show that using at least two new spectral line indices defined and measured on high-resolution ($R=6000$) spectra of a signal-to-noise ratio ($S/N \geq 10$) one gets unambiguous estimates of the age and metallicity of intermediate to old stellar populations. Spectroscopic data retrieved with new astronomical facilities, e.g., X-shooter, MEGARA, and MOSAIC, can be employed to infer the physical parameters of the emitting source by means of spectral line index and index-index diagram analysis.

Keywords: Astronomical methods: data analysis

1. INTRODUCTION

New astronomical facilities allow us to obtain stellar spectra at very high resolution. Therefore, it becomes necessary to develop new methods or update existing tools used to study low-resolution spectra and render them useful for analyzing the data provided by the new instru-

ments. One of the tools most frequently used in the analysis of spectroscopic data is the study of spectral line indices.

The use of spectral lines to understand the physical properties of stars and stellar populations started in the late 1960s of the past century (see Spinrad & Taylor 1969; Mould 1978; Faber et al. 1985; Buzzoni et al. 1992; Chavez et al. 1996). The work carried out during two decades by astronomers at Lick Observatory led to the definition of a set of 21

spectral line indices (see [Worthey et al. 1994](#); [Worthey, & Ottaviani 1997](#); [Trager et al. 1998](#)) which has been widely used to study stars, star clusters, and galaxies ([Parikh et al. 2019](#); [Sharina & Shimansky 2019](#)). The Lick set of indices was defined using spectra of the highest resolution available at the time ($\sim 8 \text{ \AA}$), each index being $\sim 30 \text{ \AA}$ wide, making them immune to dust effects. However, the age-metallicity degeneracy cannot be easily avoided ([Rose 1985](#); [Proctor, & Sansom 2002](#); [Kaviraj et al. 2007](#)). In general, inside the 30 \AA width defining each index there are several spectral features that behave in different ways as a function of time and metallicity, preventing the Lick indices from breaking this degeneracy ([Worthey 1994](#)). In fact, the strength of each spectral line is under the effect of the age-metallicity degeneracy. Index–index diagrams have helped to overcome degeneracy problems; for example, these diagrams separated effects due to the overabundance of α -elements from effects due to stellar parameters, such as T_{eff} , $\log g$, $[\text{Fe}/\text{H}]$, ξ (see [Franchini et al. 2004](#)); [Jones & Worthey \(1995\)](#) found that the $H\gamma_{\text{HR}}\text{--Fe}4668$ diagram can be used to break the age-metallicity degeneracy in old stellar populations. Unfortunately, the $H\gamma$ spectral line can be affected by emission producing unsatisfactory results (see [Gibson et al. 1999](#)).

In this Letter, we explore a high-resolution ($R= 6000$) simple stellar population (SSP) theoretical spectral energy distribution (SED) library searching for spectral indices useful for estimating the age and metallicity of stellar populations, and determine the signal-to-noise ratio (S/N) required of the observed spectrum of an intermediate-old ($> 100 \text{ Myr}$) stellar population for our method to work. The structure of this Letter is as follows. In §2 we describe the library of SSP models. In §3 we present new spectral indices and establish their reliability to infer the

age and metallicity of stellar populations. In §4 we discuss the results of our work.

2. THEORETICAL MODELS

In a separate paper ([P. R. T. Coelho et al. 2020](#), in preparation, hereafter CBC20) we present a library of high-resolution SEDs of SSPs based on the PARSEC stellar evolutionary tracks ([Bressan et al. 2012](#); [Chen et al. 2015](#)) and the [Coelho \(2014\)](#) synthetic stellar spectral library (see also [Coelho et al. 2020](#)). The [Coelho \(2014\)](#) library covers the atmospheric parameter space from $\log T_{\text{eff}} = 3.5$ to 4.3 , $\log g = -0.5$ to 5.5 , and $0.0017 \leq Z \leq 0.049$. For our purposes, three important characteristics of this library are (*a*) its high spectral resolution ($R= 20,000$), (*b*) its wavelength coverage from 2500 to 9000 \AA , and (*c*) its wavelength sampling with step $\Delta\lambda = 0.02 \text{ \AA}$. In the CBC20 models, the time scale spans from 1 Myr to 15 Gyr , with a varying time step. All of these characteristics render the CBC20 models optimal for the development of tools necessary for the analysis of data obtained with high-resolution spectrometers like X-shooter ([Vernet et al. 2011](#)), MEGARA ([Carrasco et al. 2018](#)) and MOSAIC ([Jagourel et al. 2018](#)). For our analysis, we select three CBC20 models: a metal poor α -enhanced ($[\alpha/\text{Fe}] = 0.4$) model, with constant iron abundance $[\text{Fe}/\text{H}] = -1.0$ (enhancement weighted metallicity $Z = 0.0035$, m10p04 in [Coelho 2014](#)'s notation), and two scaled solar models: one for solar metallicity ($[\text{Fe}/\text{H}] = 0.0$, $Z = 0.017$, p00p00) and a metal rich one ($[\text{Fe}/\text{H}] = 0.2$, $Z = 0.026$, p02p00).

3. SPECTRAL LINE INDICES

We carefully inspected the SSP models, looking for strong atomic lines present in the spectra of stellar populations older than 100 Myr that are clearly distinguishable in the blue part of the spectrum ($3655\text{--}5200 \text{ \AA}$). We chose this wavelength range because it is more populated by atomic lines and it is easily accessible to in-

Table 1. New indices defined following the Lick/IDS index definition (see text).

Line	Index ID	Blue Band Å	Index Å	Red Band Å	Type
Ca 3933.66	Ca3934	3906.0 – 3912.0	3926.6 – 3940.6	3948.0 – 3954.0	EW (Å)
Fe 4045.81	Fe4045	4036.0 – 4041.0	4044.8 – 4046.8	4052.0 – 4057.0	EW (Å)
Mg 4481.13	Mg4480	4473.0 – 4478.0	4480.8 – 4481.9	4484.0 – 4489.0	EW (Å)

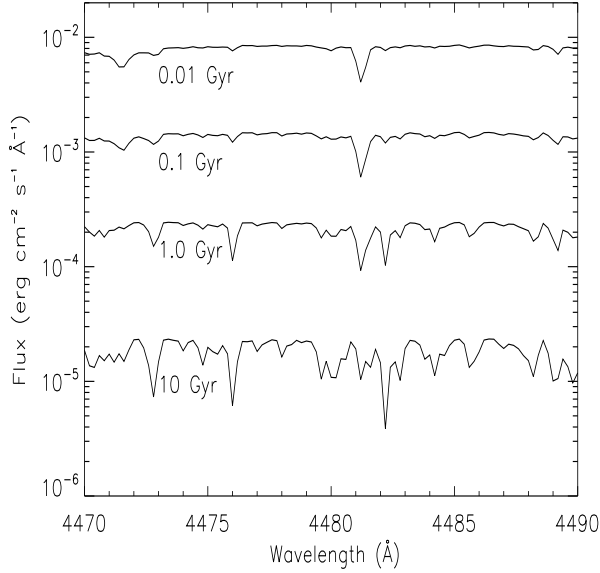


Figure 1. Change of the Mg 4481.13 Å line with age in our solar metallicity model.

struments mounted on ground-based telescopes. To carry out our analysis, we degraded and rebinned the theoretical SEDs to approximate instrumental properties of last-generation astronomical devices, e.g., $R=6000$, $\Delta\lambda = 0.2 \text{ \AA}$. We identified several spectral lines that can be useful to study stellar populations. In this work, we will concentrate on the Ca 3933.66, Fe 4045.81 and the Mg 4481.13 Å lines. We follow the standard Lick index rules (Trager et al. 1998) to define three new indices, Ca3934, Fe4045, and Mg4480. Each index involves a spectral line

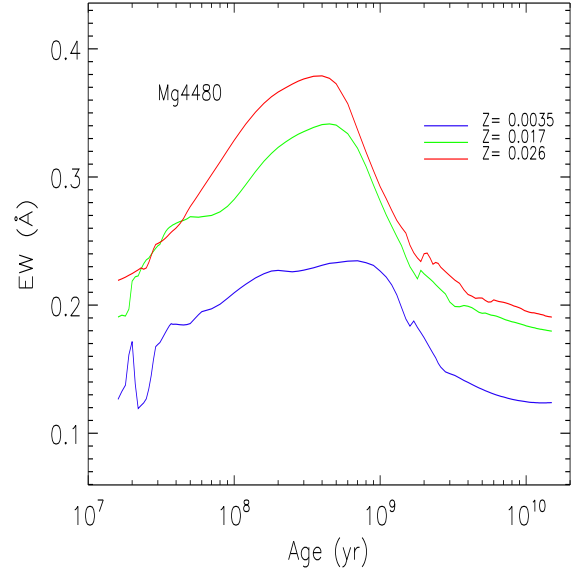


Figure 2. Behavior of Mg4480 with age and metallicity.

that is measured by its equivalent width

$$EW = \int_{\lambda_1}^{\lambda_2} \left(1 - \frac{F_{I\lambda}}{F_{C\lambda}} \right) d\lambda, \quad (1)$$

where λ_1 and λ_2 are the limits of the wavelength interval where the index is defined, and $F_{I\lambda}$ and $F_{C\lambda}$ are the spectral feature and the continuum fluxes, respectively. The continuum flux is calculated by linear interpolation of mean fluxes of the pseudo-continua F_p in bands of around 5 Å width in the blue and red sides of the main band. The pseudo-continuum is given by

$$F_p = \frac{1}{\lambda_2 - \lambda_1} \int_{\lambda_1}^{\lambda_2} F_\lambda d\lambda, \quad (2)$$

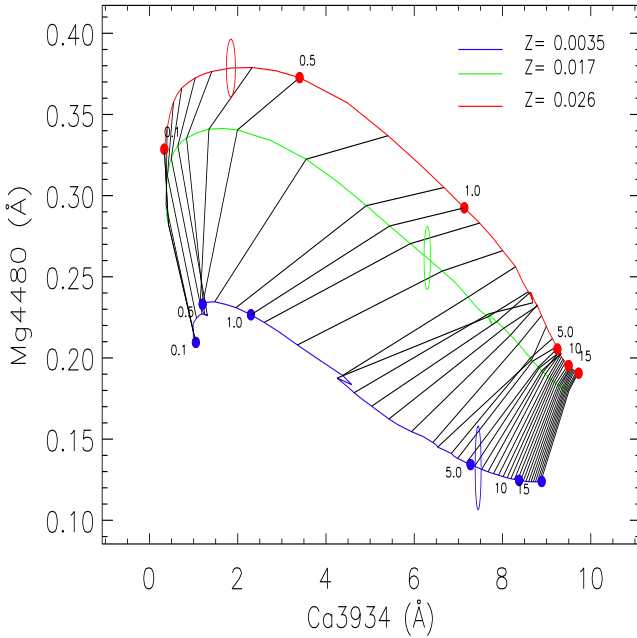


Figure 3. Ca3934–Mg4480 index–index diagram. Red, green, and blue lines correspond to metal rich, solar metallicity and metal poor models, respectively. Numbers close to the dots indicate the age of the models in Gyr. The ellipses indicate the distributions of values estimated from the simulated observations for $S/N = 10$ (see the text).

where λ_1 and λ_2 limit the wavelength interval defining the pseudo-continuum. In general, λ_1 and λ_2 are located close to the index, where there are no strong spectral lines. Table 1 lists the name of the index, the limits of the bands used to measure the index, and the pseudo-continua and the index type.

Figures 1 and 2 show, respectively, the behavior in time of the Mg 4481.13 Å line in our solar metallicity model and the Mg4480 index¹ for different metallicity models. An in-

¹ The strength of this index shows a peculiar behavior, increasing first and then decreasing. Instead, for the other two indices in Table 1 the strength of the index increases monotonically with time. Strictly speaking the CBC20 models are more reliable for age ≥ 30 Myr, due

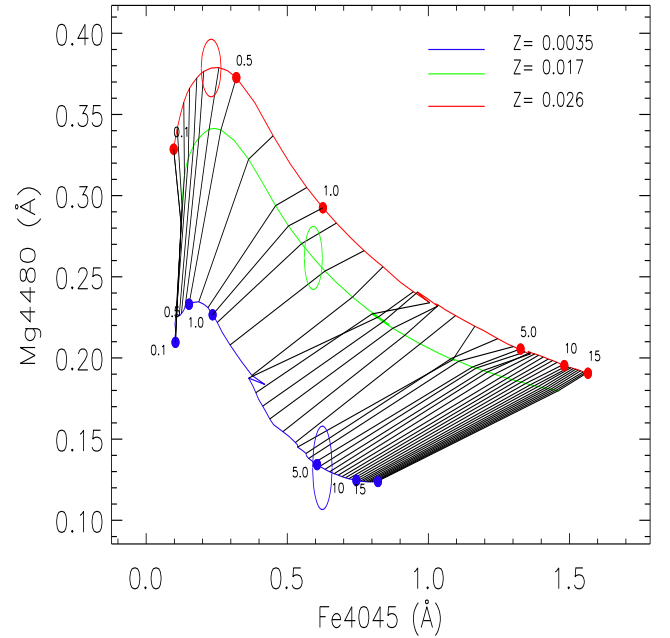


Figure 4. Same as Figure 3 but for the Fe4045–Mg4480 index–index diagram.

dex by itself is not useful to infer the age and the metallicity of an observed stellar population, since in all cases the indices suffer from the age-metallicity degeneracy; i.e., the value of the index for a young metal rich population can equal that for old metal poor population. Two index–index diagrams can be built with our three indices that prove useful for estimating age and metallicity. Figures 3 and 4 show the Ca3934–Mg4480 and the Fe4045–Mg4480 index–index diagrams, respectively. In these diagrams the two-dimensional grids indicate the change of the indices with age and metallicity. Points on the grid will have a unique associated age and metallicity.

To test the effectiveness of the index–index diagrams in determining the age and metallicity

to the coverage of the stellar library. Below this age there are some simplifications involved, and features at early ages as seen in Figure 2 maybe an artifact.

Table 2. Fit results.

Index–Index Diagram	Mock Population			S/N = 100		S/N = 10	
	ID	Age (Gyr)	Z	Age (Gyr)	$Z\%$	Age (Gyr)	$Z\%$
Ca3934–Mg4480	o-mp	5.50	0.0035	5.50 ± 0.08	100	5.58 ± 0.19	100
	i-sm	1.20	0.017	1.20 ± 0.02	100	1.20 ± 0.27	89.3
	y-mr	0.35	0.026	0.35 ± 0.02	100	0.41 ± 0.07	54.6
Fe4045–Mg4480	o-mp	5.50	0.0035	5.48 ± 0.10	100	5.45 ± 0.97	100
	i-sm	1.20	0.017	1.20 ± 0.02	100	1.16 ± 0.08	87.2
	y-mr	0.35	0.026	0.35 ± 0.02	100	0.35 ± 0.07	77.2

of stellar populations, we perform the following experiment. We select three spectra from the CBC20 models for a physically motivated combination of age and metallicity: (a) an old metal poor population of age 5.5 Gyr from the $Z=0.0035$, $[\alpha/\text{Fe}]=0.4$ model (hereafter o-mp), (b) an intermediate age solar metallicity population of age 1.2 Gyr from the $Z=0.017$ model (hereafter i-sm), and (c) a young metal rich population of age 0.35 Gyr from the $Z=0.026$ model (hereafter y-mr). Figure 5 shows the behavior of the selected spectra near the Mg4480 line.

We mimic observed spectra by adding Gaussian random noise to the flux with standard deviation $\sigma(\lambda)$ such that the resulting S/N = 10, 13.3, 20, 40, and 100 at all wavelengths, performing 1000 realizations per S/N. Then we measure the spectral indices in the mock observations. Each pair of indices leads to a problem point in the index–index diagrams of Figures 3 and 4. To this point we associate the (age, metallicity) of the model at the closest corner in the corresponding grid. In general, if the problem point falls in a region where the mesh is well separated, as it happens for the constant Z lines, we recover the true value. The distributions of our estimates for S/N = 10 are indicated in Figures 3 and 4 by ellipses. The mean values define the centers of the ellipses and the standard deviations their axes. Table 2 lists our results for S/N= 100 and 10. The values in the columns

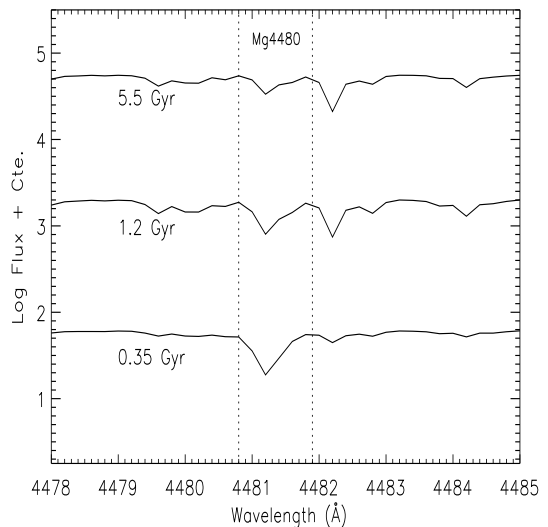


Figure 5. Behavior of the Mg4480 line (inside dotted lines) with age and metallicity. SEDs for $Z=(0.0035, 0.017, 0.026)$ at age= (5.5, 1.2, 0.35) Gyr, respectively, are shown.

marked $Z\%$ represent the percentage of the time that we recover the true Z . In the S/N = 100 case, our estimates are very close to the true values. For S/N = 10 our estimates agree with the true values within errors. We conclude that the (age, Z) estimates obtained from both index–index diagrams are quite close to the true values and that these diagrams provide a promising tool to determine these parameters.

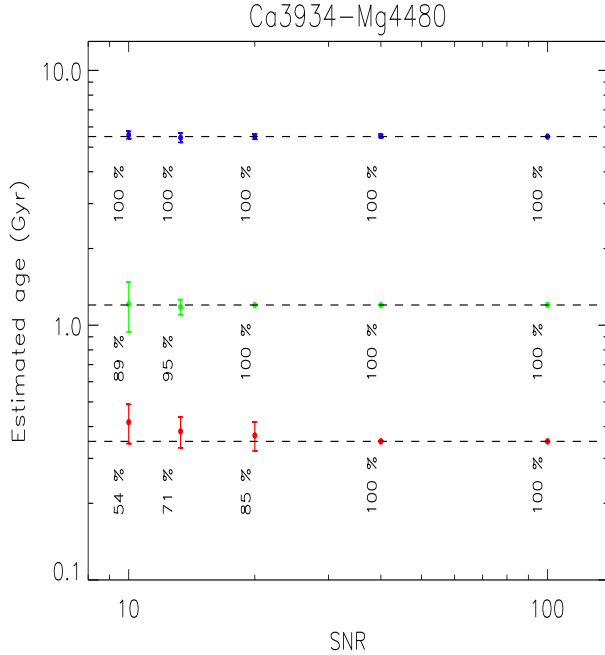


Figure 6. Age estimates from the Ca3934–Mg4480 index–index diagram vs. the S/N of the mock observations for the o-mp (blue), i-sm (green), and y-mr (red) populations. Dashed lines represent the true age. The percentage of results providing the true Z are indicated.

Figures 6 and 7 show the behavior of our age estimates from the Ca3934–Mg4480 and Fe4045–Mg4480 index–index diagrams with S/N, respectively. For large SNR, the uncertainty in the estimated age is very small, but it increases considerably for low S/N.

For comparison, we repeat our tests using the full set of 21 Lick spectral indices. The model SEDs were degraded to a resolution with $\text{FWHM} = 3 \text{ \AA}$ and resampled to $\Delta\lambda = 1.0 \text{ \AA}$. We added Gaussian random noise to the 0.35 Gyr SED to mimic an observed spectrum. We measured the indices using the most up-to-date wavelength definitions² and found a few index–index diagrams that might be used to estimate

² <http://astro.wsu.edu/worthey/html/index.table.html>

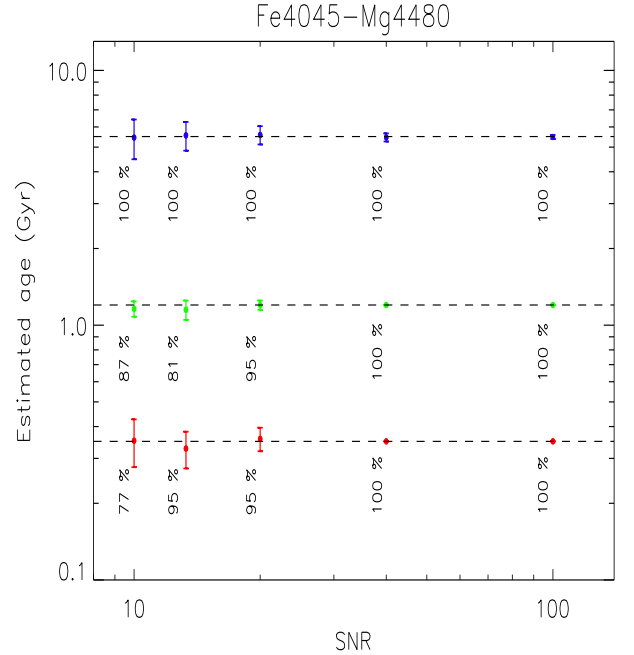


Figure 7. Same as Figure 6 but for the Fe4045–Mg4480 index–index diagram.

the basic parameters of intermediate- to old-age stellar populations. Figure 8 displays the G4300–Fe5270 index–index diagram. The ellipses correspond to the distributions of our estimates for the S/N = 10 case. The uncertainty in the estimated age grows so quickly with decreasing S/N that the true values are recovered only for the highest S/N (100).

4. DISCUSSION

We analyze a library of theoretical SEDs calculated at high resolution with the goal of identifying spectral features that can be used to determine the basic parameters of intermediate to old stellar populations. We define three new spectral indices in the blue part of the spectrum, which proved useful for simultaneously estimating age and Z for stellar populations older than 100 Myr. To test the efficiency of this tool we simulate thousands of spectroscopic observations by adding Gaussian random noise to model SEDs of intermediate to old age and dif-

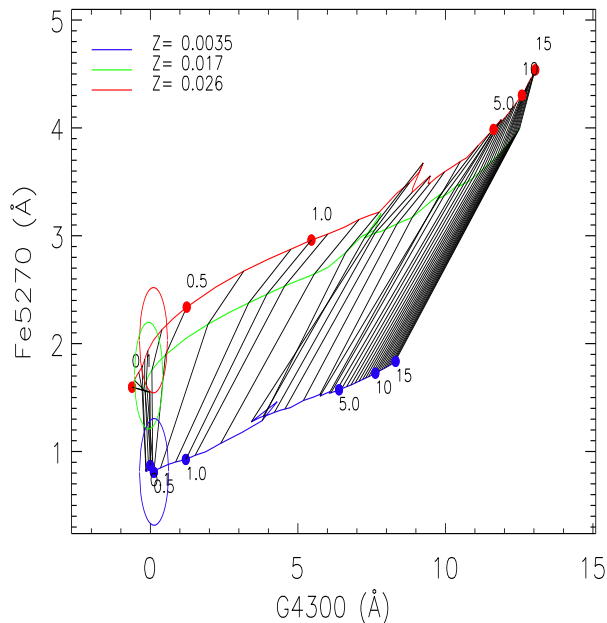


Figure 8. Same as Figure 3 but for the Lick G4300–Fe5270 index–index diagram obtained from degraded and rebinned model SEDs (see the text).

ferent Z . The new spectral indices measured on each mock spectrum were used in conjunction with the new index–index diagrams to estimate age and Z for the mock population. We find that for $S/N \geq 10$ we recover age and Z with relatively high accuracy. The new index–index diagrams allow to break the age–metallicity degeneracy present in stellar populations, as long as the indices are measured in high-resolution SEDs ($R=6000$) of $S/N \geq 10$.

A similar analysis was performed employing the full set of 21 Lick indices. We find that in this case the uncertainty in the recovered age and Z grows so quickly with decreasing S/N that parameter estimates are reliable only for the highest S/N (100 in our tests).

It is important to keep in mind that each pair of spectral indices displays a particular distribution in an index–index diagram. Therefore, some indices are useful to estimate parameters of intermediate-age populations, while other indices are more suitable for old populations. Here we report results for a limited number of indices and index–index diagrams; having both Ca, Mg and Fe indices we show that the age and metallicity estimated do not strongly depend on the α -enhanced elements abundances. In a forthcoming paper we will describe a larger set of spectral indices and index–index diagrams in the 3655–5200 Å wavelength range. These indices can be used to estimate the basic parameters of intermediate to old stellar populations.

5. ACKNOWLEDGEMENTS

We thank the anonymous referee for a quick review of this manuscript. Y.D.M. thanks CONACyT for the research grant CB-A1-S-25070. G.B. acknowledges financial support from the National Autonomous University of Mexico (UNAM) through grant DGAPA/PAPIIT IG100319 and from CONACyT through grant CB2015-252364. P.C. acknowledges support from Conselho Nacional de Desenvolvimento Científico e Tecnológico (CNPq 310041/2018-0). P.C. and G.B. acknowledge support from Fundação de Amparo à Pesquisa do Estado de São Paulo through projects FAPESP 2017/02375-2 and 2018/05392-8. P.C. and S.C. acknowledge support from USP-COFECUB 2018.1.241.1.8-40449YB. A.G.d.P. acknowledges financial support from the Spanish MCIUN under grant no. RTI2018-096188-B-I00

REFERENCES

Bressan, A., Marigo P., Girardi L., Salasnich B., Dal Cero C., Rubele S., Nanni A., et al., 2012, MNRAS, 427, 127

Buzzoni, A., Gariboldi, G., & Mantegazza, L., et al., 1992, AJ, 103, 1814

- Carrasco, E., Gil de Paz, A., Gallego, J., et al., 2018, SPIE, 1070216
- Chavez, M., Malagnini, M.L., & Morossi, C., 1996, ApJ, 471, 726
- Chen H.-L., Woods T. E., Yungelson L. R., Gilfanov M., Han Z., et al., 2015, MNRAS, 453, 3024
- Coelho, P.R.T., 2014, MNRAS, 440, 1027
- Coelho, P. R. T., Bruzual, G., & Charlot, S. 2020, MNRAS, 491, 2025
- Faber, S.M., Friel, E. D., Burstein, D., & Gaskell, C. M., et al., 1985, ApJS, 57, 711
- Franchini, M., Morossi, C., Di Marcantonio, P., et al., 2004, ApJ, 601, 485
- Gibson, B. K., Madgwick, D. S., Jones, L. A., et al. 1999, AJ, 118, 1268
- Jagourel, P., Fitzsimons, E., Hammer, F., et al., 2018, SPIE 10702A4
- Jones, L. A., & Worthey, G. 1995, ApJL, 446, L31
- Kaviraj, S., Rey, S.-C., Rich, R. M., et al., 2007, MNRAS, 381, L74
- Mould, J.R. 1978, ApJ, 220, 434
- Parikh, T., Thomas, D., Maraston, C., et al., 2019, MNRAS, 483, 3420
- Proctor, R. N., & Sansom, A. E. 2002, MNRAS, 333, 517
- Rose, J. A. 1985, AJ, 90, 1927
- Sharina, M.E., & Shimansky, V.V., 2019, ARep, 63, 687
- Spinrad, H., & Taylor, B. J. 1969, ApJ, 157, 1279
- Trager, S. C., Worthey, G., Faber, S. M., et al., 1998, ApJS, 116, 1
- Vernet, J., Dekker, H., D’Odorico, S., et al., 2011, A&A, 536, A105
- Worthey, G. 1994, ApJS, 95, 107
- Worthey, G., Faber, S. M., Gonzalez, J. J., & Burstein, D. et al., 1994, ApJS, 94, 687
- Worthey, G., & Ottaviani, D.L. 1997, ApJS, 111, 377